

Polyoxometalate modified transparent metal selenide counter electrodes for high-efficiency bifacial dye-sensitized solar cells

*Lu Zhang,^a Weichao Chen,^{*a} Ting Wang,^a Yunjiang Li,^a Chunhui Ma,^a Yuxiao Zheng^a
and Jian Gong^{*a}*

^aKey Laboratory of Polyoxometalate and Reticular Material Chemistry of Ministry of Education, Department of Chemistry, Northeast Normal University, Changchun, Jilin 130024, China

Email: chenwc061@nenu.edu.cn

Table of Contents

Figure S1. Full XPS spectra of (a) $\text{Co}_{0.85}\text{Se}$; High-resolution XPS spectra of (b) P 2p of $\text{PW}_{11}\text{Co}/\text{Co}_{0.85}\text{Se}$

Figure. S2 EDX spectra of $\text{PW}_{11}\text{Co}/\text{Co}_{0.85}\text{Se}$

Figure S3 EDX elemental mapping of Co, Se, P, W and O in $\text{PW}_{11}\text{Co}/\text{Co}_{0.85}\text{Se}$

Figure S4 TEM images of $\text{PW}_{11}\text{Co}/\text{Co}_{0.85}\text{Se}$

Figure S5 IR, XRD, and transparency images of the $\text{PW}_{11}\text{Co}/\text{Co}_{0.85}\text{Se}$ catalyst before and after the test

Figure S6 SEM of $\text{PW}_{11}\text{Co}/\text{Co}_{0.85}\text{Se}$ CE before and after durability test

Figure S7 Elemental mapping of Co, Se, P, W and O in $\text{PW}_{11}\text{Co}/\text{Co}_{0.85}\text{Se}$ after durability test

Figure S8 Bode curves of Pt, $\text{Co}_{0.85}\text{Se}$, $\text{PW}_{11}\text{Co}-0.3/\text{Co}_{0.85}\text{Se}$, $\text{PW}_{11}\text{Co}-0.5/\text{Co}_{0.85}\text{Se}$, and $\text{PW}_{11}\text{Co}-0.8/\text{Co}_{0.85}\text{Se}$ CEs

Figure. S9 Long-term stability of DSSCs based on $\text{PW}_{11}\text{Co}/\text{Co}_{0.85}\text{Se}$

Figure. S10 CV curves of $\text{PW}_{11}\text{Co}/\text{Co}_{0.85}\text{Se}$ electrode subjected to aging for some days at room temperature

Figure. S11 Nyquist plot of $\text{PW}_{11}\text{Co}/\text{Co}_{0.85}\text{Se}$ electrode subjected to aging for some days at room temperature

Figure. S12 Tafel of $\text{PW}_{11}\text{Co}/\text{Co}_{0.85}\text{Se}$ electrode subjected to aging for some days at room temperature.

Figure. S13 (a) Cyclic voltammetry curve of PW_{11}Co (1 mol L^{-1} KCl solution at pH=7). (b) A plot of Kubelka–Munk function F against energy E of PW_{11}Co .

Table S1 EIS parameters using the different materials as CE

Table S2 Photovoltaic parameters of the DSSCs assembled with other CEs

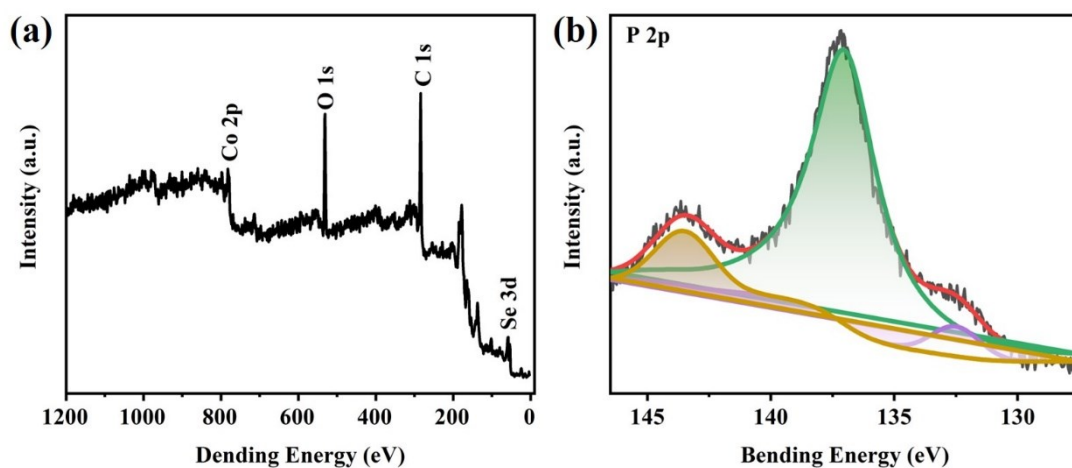


Figure S1 Full XPS spectra of (a) $\text{Co}_{0.85}\text{Se}$; High-resolution XPS spectra of (b) P 2p of $\text{PW}_{11}\text{Co}/\text{Co}_{0.85}\text{Se}$.

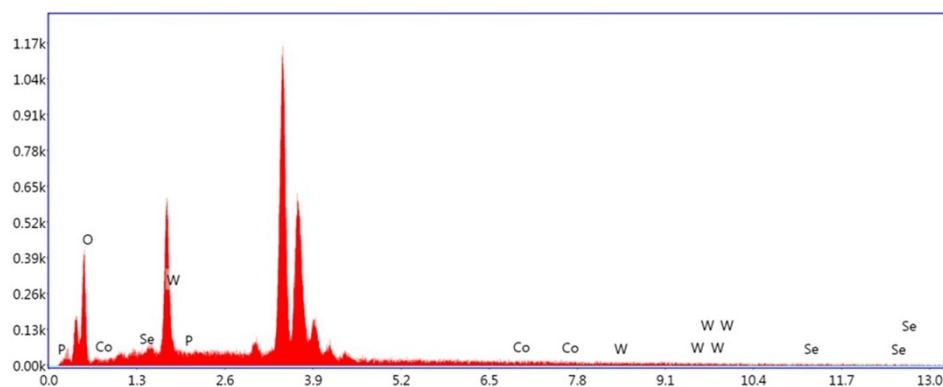


Figure. S2 EDX spectra of $\text{PW}_{11}\text{Co}/\text{Co}_{0.85}\text{Se}$.

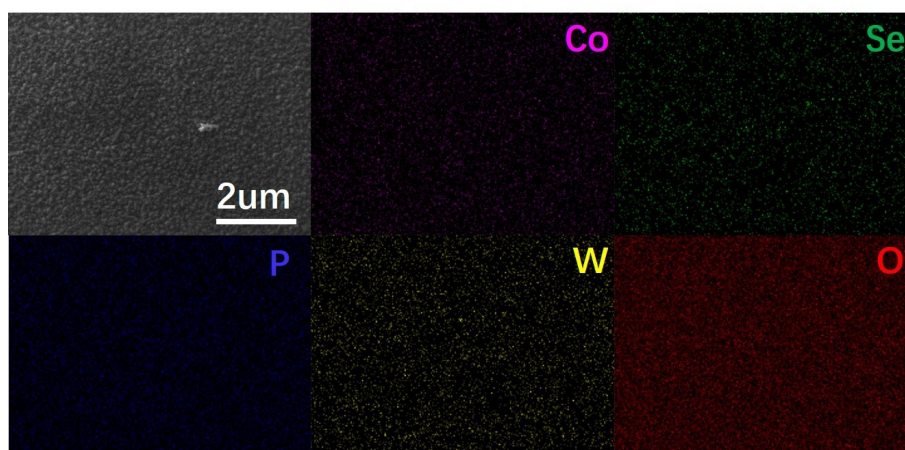


Figure S3 EDX elemental mapping of Co, Se, P, W and O in $\text{PW}_{11}\text{Co}/\text{Co}_{0.85}\text{Se}$.

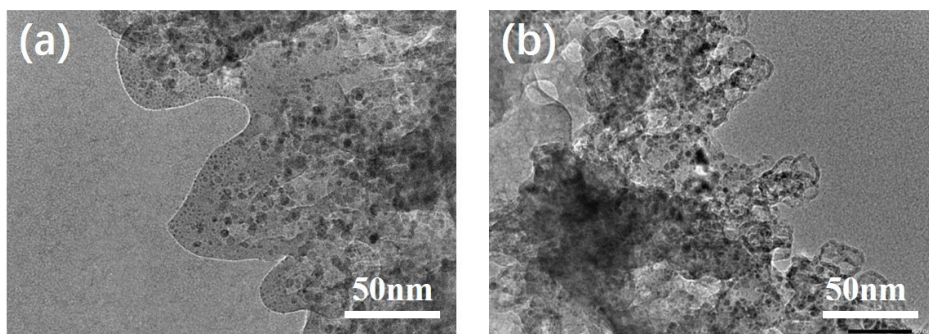


Figure S4 TEM images of $PW_{11}Co/Co_{0.85}Se$.

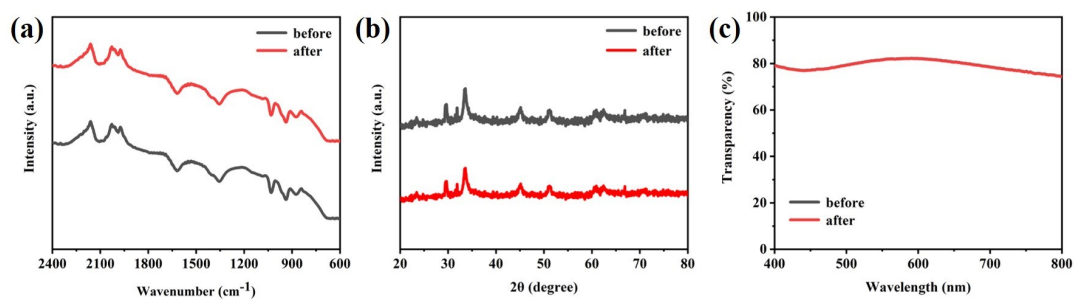


Figure S5 The IR, XRD and optical transmittance spectra of the $PW_{11}Co/Co_{0.85}Se$ CE after the durability tests.

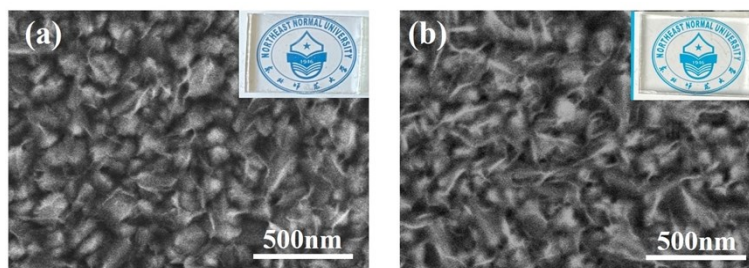


Figure S6 SEM of $PW_{11}Co/Co_{0.85}Se$ CE before and after durability test.

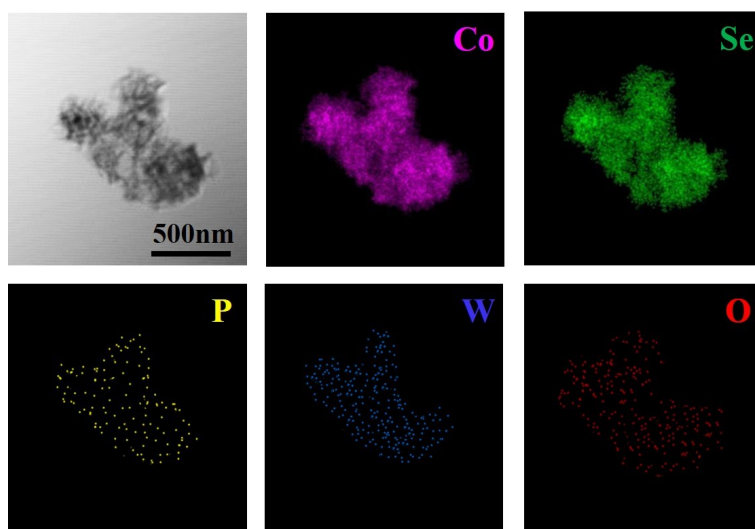


Figure S7 Elemental mapping of Co, Se, P, W and O in $PW_{11}Co/Co_{0.85}Se$ after durability test.

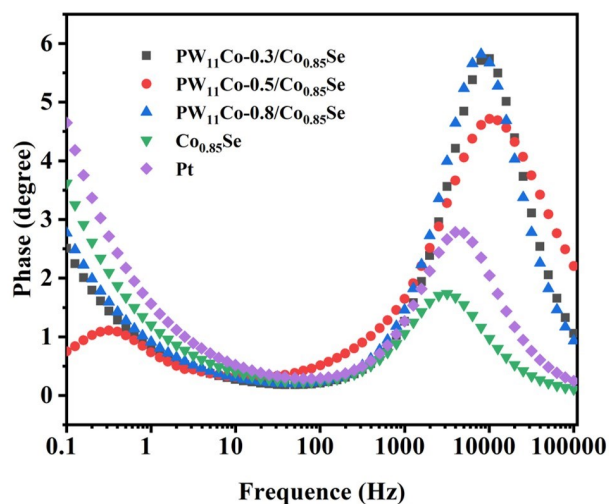


Figure S8 Bode curves of Pt, Co_{0.85}Se, PW₁₁Co-0.3/Co_{0.85}Se, PW₁₁Co-0.5/Co_{0.85}Se, and PW₁₁Co-0.8/Co_{0.85}Se CEs.

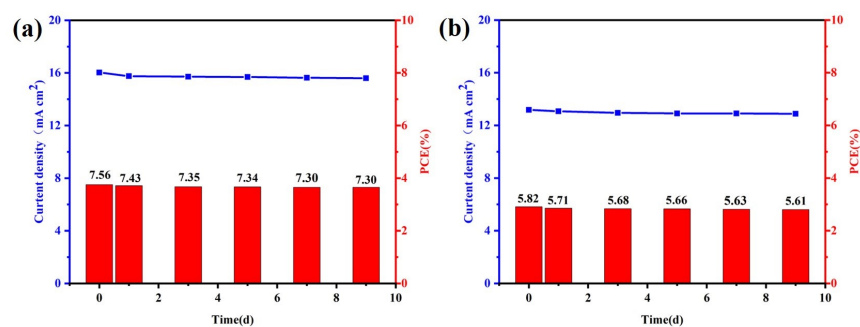


Figure. S9 Long-term stability of DSSCs based on PW₁₁Co/Co_{0.85}Se.

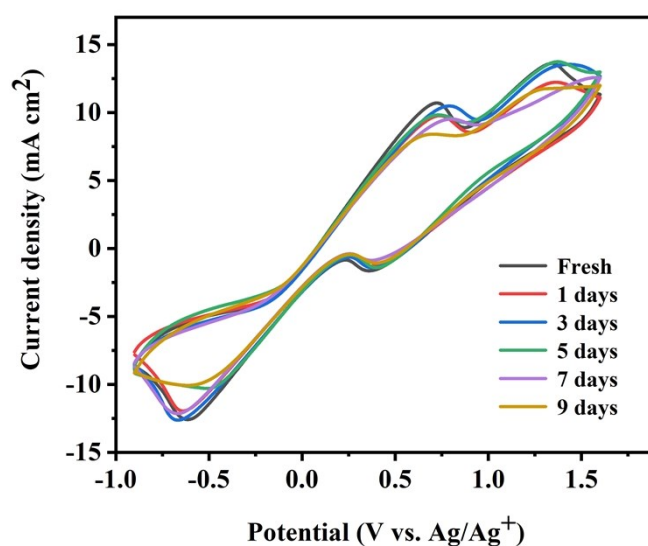


Figure. S10 CV curves of PW₁₁Co/Co_{0.85}Se electrode subjected to aging for some days at room temperature.

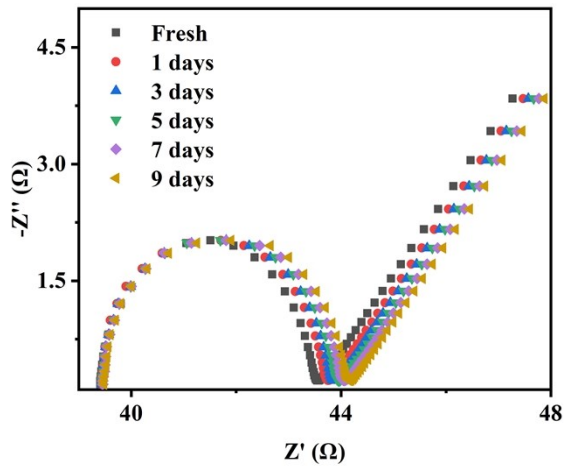


Figure. S11 Nyquist plot of $PW_{11}Co/Co_{0.85}Se$ electrode subjected to aging for some days at room temperature.

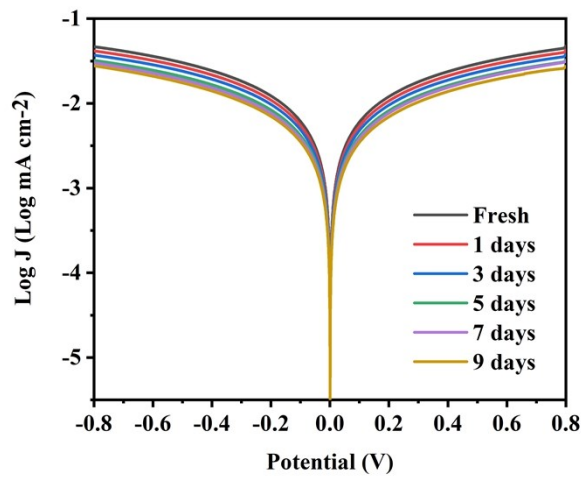


Figure. S12 Tafel of $PW_{11}Co/Co_{0.85}Se$ electrode subjected to aging for some days at room temperature.

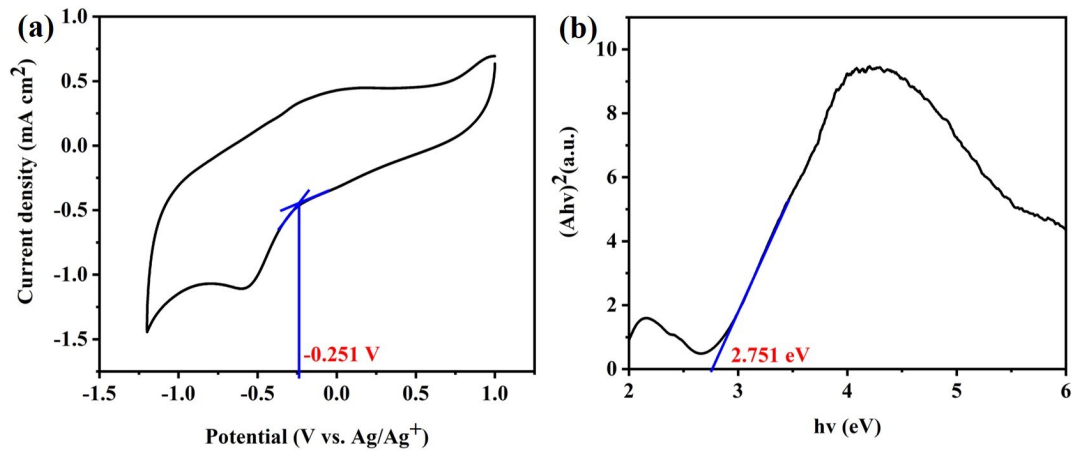


Figure. S13 (a) Cyclic voltammogram curve of $PW_{11}Co$ (1 mol L^{-1} KCl solution at $\text{pH}=7$). (b) A plot of Kubelka–Munk function F against energy E of $PW_{11}Co$.

Cyclic Voltammetry (CV) is widely used to study the electrochemical characteristics of materials. The first reduction peak of the CV curve is used to estimate the LUMO energy level of $PW_{11}Co$.^[16] The value of the abscissa relative to the Ag/AgCl standard electrode is -0.251 V, which is converted to a standard hydrogen electrode of -0.054 V, and converted to a vacuum energy level, that is, the LUMO energy level is -4.45 eV. Solid diffuse reflection is used to estimate the bandwidth of $PW_{11}Co$. We use the Kubelka–Munk function F to plot the energy E of $PW_{11}Co$.^[16] The energy axis and the extrapolation line of the linear region of the absorption edge intersect at a certain point whose quantitative value is the E_g of $PW_{11}Co$, so the E_g of $PW_{11}Co$ is estimated to be 2.751 eV.

Table S1. EIS parameters using the different materials as CEs.

| Sample | $R_s(\Omega/cm^2)$ | $R_{ct}(\Omega/cm^2)$ | $Z_w(\Omega/cm^2)$ |
|------------------------------|--------------------|-----------------------|--------------------|
| 0.3- $PW_{11}Co/Co_{0.85}Se$ | 35.08 | 7.83 | 0.45 |
| 0.5- $PW_{11}Co/Co_{0.85}Se$ | 39.40 | 4.02 | 0.23 |
| 0.8- $PW_{11}Co/Co_{0.85}Se$ | 35.93 | 8.09 | 0.39 |
| $Co_{0.85}Se$ | 34.94 | 7.65 | 0.47 |
| Pt | 41.23 | 2.56 | 0.31 |

Table S2. Photovoltaic parameters of the DSSCs assembled with other CEs.

| CEs | irradiation | V_{oc} / mV | J_{sc} / mA cm^{-2} | FF | $PCE / \%$ | Ref. |
|----------------------------------|-------------|---------------|----------------------------|------|------------|------|
| $Co_{0.85}Se$ nanotubes | front | 706 | 14.51 | 0.52 | 5.34 | (1) |
| $Co_{0.85}Se$ nanoparticles | front | 660 | 13.44 | 0.68 | 6.03 | (2) |
| Co- $Co_{0.85}Se$ | front | 650 | 14.73 | 0.68 | 6.55 | (3) |
| $Co_{0.85}Se/RGO$ | front | 706 | 16.01 | 0.69 | 7.81 | (4) |
| CuCoSe | front | 680 | 10.61 | 0.74 | 5.38 | (5) |
| Polycrystalline $Co_{0.85}Se$ | front | 716 | 15.85 | 0.69 | 7.87 | (6) |
| CoSe | front | 690 | 15.60 | 0.66 | 6.79 | (7) |
| $Ni_{0.85}Se$ nanospheres | front | 760 | 13.2 | 0.68 | 6.82 | (8) |
| PVP | front | 570 | 20.32 | 0.46 | 5.45 | (9) |

| | | | | | | |
|---|-------|-----|-------|------|------|-----------|
| (4w%)/PANI | rear | 550 | 19.08 | 0.43 | 4.66 | |
| RuSe | front | 729 | 12.17 | 0.73 | 6.51 | (10) |
| | rear | 681 | 3.64 | 0.74 | 1.84 | |
| PtNP-EMTE | front | 700 | 11.63 | 0.68 | 5.67 | (11) |
| | rear | 700 | 9.98 | 0.67 | 4.87 | |
| Pt-Mo ₂ C | front | 710 | 15.61 | 0.67 | 7.4 | (12) |
| | rear | 700 | 12.00 | 0.66 | 5.5 | |
| PVP(4wt%)/PAN I | front | 570 | 20.32 | 0.46 | 5.45 | (13) |
| | rear | 550 | 19.05 | 0.43 | 4.66 | |
| 16nm-MoS ₂ | front | 714 | 13.96 | 0.69 | 6.88 | (14) |
| | rear | 689 | 6.67 | 0.72 | 3.31 | |
| Zn-TCPP-Pt | front | 690 | 12.95 | 0.61 | 5.48 | (15) |
| | rear | 690 | 10.93 | 0.63 | 4.88 | |
| PW ₁₁ Co/Co _{0.85} Se | front | 830 | 15.94 | 0.60 | 7.51 | This work |
| | rear | 730 | 13.33 | 0.60 | 5.79 | |

References

- (1) H. Yuan, Q. Z. Jiao, J. Liu, X. F. Liu, Y. J. Li, D. X. Shi, Q. Wu, Y. Zhao and H. S. Li, Facile synthesis of Co_{0.85}Se nanotubes/reduced graphene oxide nanocomposite as Pt-free counter electrode with enhanced electrocatalytic performance in dye-sensitized solar cells, *Carbon*, 2017, **122**, 381-388.
- (2) Q. S. Jiang and G. Hu, Co_{0.85}Se hollow nanoparticles as Pt-free counter electrode materials for dye-sensitized solar cells, *Mater. Lett.*, 2015, **153**, 114-117.
- (3) L. Chen, H. X. Yin, Y. Zhou, H. Dai, T. Yu, J. G. Liua, and Z. G. Zou, In situ direct growth of single crystalline metal (Co, Ni) selenium nanosheets on metal fibers as counter electrodes toward low-cost, high-performance fiber-shaped dye-sensitized solar cells, *Nanoscale*, 2016, **8**, 2304-2308.
- (4) H. Yuan, Q. Z. Jiao, J. Liu, X. F. Liu, Y. J. Li, D. X. Shi, Q. Wu, Y. Zhao and H. S. Li, Facile synthesis of Co_{0.85}Se nanotubes/reduced graphene oxide nanocomposite as Pt-free counter electrode with enhanced electrocatalytic performance in dye-

sensitized solar cells, *Carbon*, 2017, **122**, 381-388.

- (5) P. J. Li, Q. W. Tang, Highly transparent metal selenide counter electrodes for bifacial dye-sensitized solar cell, *J. Power Sources*, 2016, **317**, 43-48.
- (6) C. Q. Feng, G. Y. Zhao, Y. R. Li, H. L. Cheng and Z. S. Wang, Single-crystal cobalt selenide nanobelt as a highly efficient cathode for stable quasi-solid-state dye sensitized solar cell, *J. Power Sources*, 2019, **426**, 16-22.
- (7) W. W. Liu, W. Jiang, Y. C. Liu, W. J. Niu, M. C. Liu, K. Zhao, L. Y. Zhang, L. Lee, L. B. Kong and Y. L. Chueh, Platinum-Free Ternary Metallic Selenides as Nanostructured Counter Electrode for High-Efficiency Dye-Sensitized Solar Cell by Interface Engineering, *ACS Appl. Energy Mater.*, 2020, **3**, 3704-3713.
- (8) X. Zhang, Y.X. Yang, S.Q. Guo, F. Z and Hu, L. Liu, Mesoporous Ni_{0.85}Se nanospheres grown in situ on graphene with high performance in dye-sensitized solar cells, *ACS Appl. Mater. Interfaces*, 2015, **7**, 8457-8464.
- (9) J. Gao, Y. Yang, Z. Zhang, J.Y. Yan, Z.H. Lin and X. Y. Guo, Bifacial quasi-solid-state dye-sensitized solar cells with Poly (vinyl pyrrolidone)/polyaniline transparent counter electrode, *Nano Energy*, 2016, **26**, 123-130.
- (10) P.Z. Yang, Q.W. Tang, Bifacial quasi-solid-state dye-sensitized solar cells with metal selenide counter electrodes, *Electrochim. Acta*, 2016, **188**, 560-565.
- (11) A. Khan, Y. T. Huang, T. Miyasaka, M. Ikegami, S. P. Feng and W. D. Li, Solution-Processed Transparent Nickel-Mesh Counter Electrode with in-Situ Electrodeposited Platinum Nanoparticles for Full-Plastic Bifacial Dye-Sensitized Solar Cells, *ACS Appl. Mater. Interfaces*, 2017, **9**, 8083-8091.
- (12) C. X. Wu, R. Li, Y. L. Wang, S. Lu, J. Lin, Y. C. Liu and X. T. Zhang, Strong metal-support interactions enable highly transparent Pt-Mo₂C counter electrodes of

bifacial dye-sensitized solar cells, *Chem. Commun.*, 2020, **56**, 10046.

(13) J. Gao, Y. Yang, Z. Zhang, J. Y. Yan, Z. H. Lin, X. Y. Guo, Bifacial quasi-solid-state dye-sensitized solar cells with Poly (vinyl pyrrolidone)/polyaniline transparent counter electrode, *Nano Energy*, 2016, **26**, 123-130.

(14) T. Jeong, S. Y. Ham, B. Koo, P. Lee, Y. S. Min, J. Y. Kim, M. J. Ko, Transparent 3 nm-thick MoS₂ counter electrodes for bifacial dye-sensitized solar cells, *J. Ind. Eng. Chem.* 2019, **80**, 106-111.

(15) Y. B. Tian, Y. Y. Wang, S. M. Chen, Z. G. Gu and J. Zhang, Epitaxial Growth of Highly Transparent Metal–Porphyrin Framework Thin Films for Efficient Bifacial Dye-Sensitized Solar Cells, *ACS Appl. Mater. Interfaces*, 2020, **12**, 1078-1083.

(16) Y. B. Tang, C. S. Lee, J. Xu, Z. T. Liu, Z. H. Chen, Z. He, Y. L. Cao, G. Yuan, H. Song, L. Chen, L. Luo, H. M. Cheng, W. J. Zhang, I. Bello, S. T. Lee, Incorporation of Graphenes in Nanostructured TiO₂ Films via Molecular Grafting for Dye-Sensitized Solar Cell Application, *ACS Nano*, 2010, **4**, 3482-3488.